Anal. Chem. **1996**, *68*, 2296−2303

Two-Dimensional Model of a Direct Current Glow Discharge: Description of the Electrons, Argon Ions, and Fast Argon Atoms

A. Bogaerts* and R. Gijbels

Department of Chemistry, University of Antwerp (UIA), Universiteitsplein 1, B-2610 Wilrijk-Antwerp, Belgium

W. J. Goedheer

FOM-Instituut voor Plasmafysica, "Rijnhuizen", P.O. Box 1207, 3430 BE Nieuwegein, The Netherlands

To improve the analytical results of techniques that use the glow discharge as spectroscopic source, a good insight into the glow discharge is desirable. This can be obtained by mathematical modeling. In this work, a two-dimensional model is developed to describe the electrons, argon ions, and fast argon atoms in a direct current glow discharge in argon. The model consists of a Monte Carlo model for the fast electrons, a Monte Carlo model for the argon ions and fast argon atoms in the cathode dark space, and a fluid model for the argon ions and slow electrons. Results in two dimensions are presented for a standard flat cell of the VG 9000 glow discharge mass spectrometer (VG Elemental, Fisons); they include the densities, mean energies, and collision rates of the plasma species, the potential distribution, and the axial and radial electric fields.

Glow discharges are gaining increasing interest as spectroscopic sources for mass spectrometry, optical emission spectrometry, and atomic absorption spectrometry.[1,2] For good analytical practice, a thorough understanding of the glow discharge is required. This can be attempted by mathematical modeling. Glow discharges have been described by different kinds of models, i.e., fluid models,[3−12] Boltzmann models,[13−15] and Monte Carlo simulations.[16−25] The Monte Carlo approach is the most accurate one, because it describes the plasma particles on the lowest microscopical level, taking explicitly into account the energy losses by collisions and the energy gain from the electric field. This is especially required for the electrons since these species are not in hydrodynamic equilibrium, which means that they gain more energy from the strong electric field in the cathode dark space than they lose by collisions. However, the Monte Carlo model on its own is not a self-consistent method, i.e., a particular electric field is applied to the discharge to calculate the transport of the charged particles, but this electric field is not necessarily the same as the one that would be obtained from the charged particle densities through the Poisson equation. Self-consistent results can, however, be achieved in so-called hybrid models.[26−34] These account for the nonequilibrium nature of the fast electrons by treating them with Monte Carlo or Boltzmann models, whereas the gas ions and slow electrons are described self-consistently with the electric field in a fluid model.

In this work, a two-dimensional self-consistent hybrid model is developed for the direct current glow discharge in argon. The electrons are split up in a fast group and a slow group. The fast electrons are described with Monte Carlo simulations, whereas the slow electrons and the argon ions are modeled with a fluid approach. Moreover, since the argon ions are not in hydrodynamic equilibrium with the strong electric field in the cathode dark space (CDS) of the glow discharge, they are also treated in this region with a Monte Carlo model, together with the fast argon atoms that are created by charge transfer and elastic collisions of the argon ions. Hence, the complete hybrid model consists of (i) a Monte Carlo model for the fast electrons in the entire discharge, (ii) a Monte Carlo model for the argon ions and fast

(1) Harrison, W. W. Glow Discharge Mass Spectrometry. In *Inorganic Mass Spectrometry*; Adams, F., Gijbels, R., Van Grieken, R., Eds.; Wiley: New York, 1988; Chapter 3.
(2) Marcus, R. K. *Glow Discharge Spectroscopies*; Plenum Press: New York, 1993.
(3) Passchier, J. D. P.; Goedheer, W. J. *J. Appl. Phys.* **1993**, *73*, 1073−1079.
(4) Passchier, J. D. P.; Goedheer, W. J. *J. Appl. Phys.* **1993**, *74*, 3744−3751.
(5) Boeuf, J. P. *Phys. Rev. A* **1987**, *36*, 2782−2792.
(6) Boeuf, J. P. *J. Appl. Phys.* **1988**, *63*, 1342−1349.
(7) Young, F. F.; Wu, C. J. *J. Appl. Phys.* **1993**, *74*, 839−847.
(8) Schmitt, W.; Kohler, W. E.; Ruder, H. *J. Appl. Phys.* **1992**, *71*, 5783−5791.
(9) Graves, D. B.; Jensen, K. F. *IEEE Trans. Plasma Sci.* **1986**, *17*, 78−91.
(10) Meyyappan, M.; Kreskovsky, J. P. *J. Appl. Phys.* **1990**, *68*, 1506−1512.
(11) Meyyappan, M.; Govindan, T. R. *J. Appl. Phys.* **1993**, *74*, 2250−2259.
(12) Belenguer, Ph.; Boeuf, J. P. *Phys. Rev. A* **1990**, *41*, 4447−4459.
(13) Carman, R. J.; Maitland, A. *J. Phys. D* **1987**, *20*, 1021−1030.
(14) Abril, I. *Comput. Phys. Commun.* **1988**, *51*, 413−419.
(15) Carman, R. J. *J. Phys. D* **1989**, *22*, 55−66.
(16) Boeuf, J. P.; Marode, E. *J. Phys. D* **1982**, *15*, 2169−2187.
(17) Hashiguchi, S. *IEEE Trans. Plasma Sci.* **1991**, *19*, 297−300.
(18) Wronski, Z. *Vacuum* **1991**, *42*, 635−644.
(19) Sun, J.; Gong, Y.; Wang, D. *J. Phys. D* **1993**, *26*, 436−441.
(20) Weng, Y.; Kushner, M. J. *Phys. Rev. A* **1990**, *42*, 6192−6200.
(21) Deleted in proof.
(22) Deleted in proof.
(23) Hashiguchi, S.; Hasikuni, M. *Jpn. J. Appl. Phys.* **1988**, *27*, 1010−1016.
(24) Li, J.; Chen, Q.-M.; Li, Z.-G. *J. Phys. D* **1995**, *28*, 681−688.
(25) Bogaerts, A.; van Straaten, M.; Gijbels, R. *Spectrochim. Acta* **1995**, *50B*, 179−196.
(26) Surendra, M.; Graves, D. B.; Jellum, G. M. *Phys. Rev. A* **1990**, *41*, 1112−1125.
(27) Tsai, J.-H.; Wu, C.-H. *J. Phys. D* **1993**, *26*, 496−499.
(28) Dexter, A. C.; Farrell, T.; Lees, M. I. *J. Phys. D* **1989**, *22*, 413−430.
(29) Sommerer, T. J.; Kushner, M. J. *J. Appl. Phys.* **1992**, *71*, 1654−1673.
(30) Schoenbach, K. H.; Chen, H.; Schaefer, G. *J. Appl. Phys.* **1989**, *67*, 154−162.
(31) Sato, N.; Tagashira, H. *IEEE Trans. Plasma Sci.* **1991**, *19*, 102−112.
(32) Boeuf, J. P.; Pitchford, L. C. *IEEE Trans. Plasma Sci.* **1991**, *19*, 286−296.
(33) Fiala, A.; Pitchford, L. C.; Boeuf, J. P. *Phys. Rev. E* **1994**, *49*, 5607−5622.
(34) Bogaerts, A.; Gijbels, R.; Goedheer, W. J. *J. Appl. Phys.* **1995**, *78*, 2233−2241.

S0003-2700(95)01065-1 CCC: $12.00

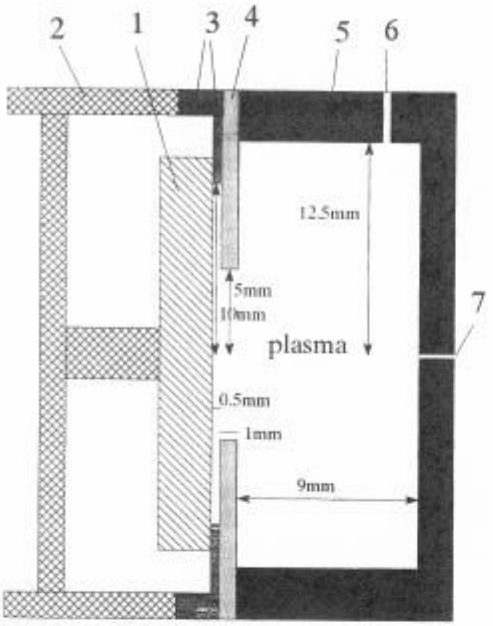

Figure 1. Schematic representation of the new standard cell for analyzing flat samples in the VG 9000 glow discharge mass spectrometer (VG Elemental, Fisons). 1, Sample (cathode); 2, sample holder (at cathode potential); 3, insulator; 4, front plate (at anode potential); 5, cell house (anode); 6, argon gas inlet; 7, exit slit to the mass spectrometer.

argon atoms in the CDS, and (iii) a fluid model for the slow electrons and argon ions in the entire discharge. These models were already developed earlier in one dimension[25,34,35] but are here extended to two dimensions (three dimensions because of cylindrical symmetry) in order to obtain the results in the complete three-dimensional geometry. Typical results include the densities, fluxes, and energies of the different plasma species and information about their collision processes, as well as the self-consistent electric field and potential distribution throughout the discharge. Results will be shown for typical discharge conditions and for a standard cell of the VG 9000 glow discharge mass spectrometer (VG Elemental, Fisons). The present results concern only the electrons, argon ions, and fast atoms (i.e., the so-called plasma species) and not yet the sputtered (analytically important) species. However, the present results are required for calculating the behavior of the sputtered species, which will be dealt with in a later work.

DESCRIPTION OF THE MODELS

A. Model Assumptions. The discharge geometry to which the models are applied is that of a standard discharge cell of the VG 9000 glow discharge mass spectrometer (VG Elemental, Fisons) for analyzing flat samples, the so-called new flat cell[36] (see Figure 1). It is, however, assumed that the glow discharge cell is in a closed configuration, without argon gas inlet and without exit slit to the mass spectrometer. This means that there is no gas flow and that the argon gas is more or less at rest, uniformly distributed throughout the cell. Besides the argon gas atoms at rest (Ar^0), the models assume that the plasma also consists of singly charged positive argon ions (Ar^+), fast argon atoms (Ar_f^0), fast electrons and slow electrons (definitions of fast and slow are given below). Species of the cathode material (copper) are in the first instance neglected, since it has been shown[37] that they are only of minor importance for the description of the discharge as such. Indeed, it is calculated that the copper atom density is 4 orders of magnitude lower than the argon atom density, and the copper ion density is found to be only a few percent of the argon ion density. Since the glow discharge cell is cylindrically symmetrical, the three-dimensional geometry can be reduced to two dimensions. The explicit treatment of the particles in the Monte Carlo models is, however, carried out in three dimensions.

B. Fast Electron Monte Carlo Model. The electrons start at the cathode with energies of 4 eV,[38] created by ion-induced secondary electron emission. The flux of electrons starting at the cathode is determined from the fluid model (see below). The electrons are followed throughout the whole three-dimensional discharge, one after the other. By following a large number of electrons, statistically valid results can be obtained. During successive timesteps (Δt), the trajectory is calculated by Newton's laws:

$$z = z_0 + v_{z_0}\Delta t + \frac{q\mathcal{E}_{ax}}{2m}(\Delta t)^2$$

$$x = x_0 + v_{x_0}\Delta t + \frac{q\mathcal{E}_{rad}\cos(\alpha)}{2m}(\Delta t)^2$$

$$y = y_0 + v_{y_0}\Delta t + \frac{q\mathcal{E}_{rad}\sin(\alpha)}{2m}(\Delta t)^2 \qquad (1)$$

$$v_z = v_{z_0} + \frac{q\mathcal{E}_{ax}}{m}\Delta t$$

$$v_x = v_{x_0} + \frac{q\mathcal{E}_{rad}\cos(\alpha)}{m}\Delta t$$

$$v_y = v_{y_0} + \frac{q\mathcal{E}_{rad}\sin(\alpha)}{m}\Delta t$$

where z_0, x_0, y_0 and z, x, y are the position coordinates before and after Δt, v_{z_0}, v_{x_0}, v_{y_0} and v_z, v_x, v_y are the velocities before and after Δt, $\mathcal{E}_{ax}$ and $\mathcal{E}_{rad}$ are the axial and radial electric fields, α is the azimuthal angle of the radial position (i.e., the angle of the radial position coordinates with respect to the x-axis), and q and m are the electron charge and mass, respectively. The probability (P) of collision during that time step is calculated with eq 2 and compared with a random number between 0 and 1:

$$P = 1 - \exp(-\Delta s n \sigma_{coll}) \qquad (2)$$

where n is the argon gas density, σ_{coll} is the total collision cross section, and Δs is the distance traveled during Δt. If the probability is lower than the random number, then no collision takes place, and the electron is followed during the next time step. If the probability is higher, a collision takes place. Collision

(35) Bogaerts, A.; Gijbels, R. *J. Appl. Phys.* **1995**, *78*, 6427–6431.
(36) Clark, J.; Greb, U.; Ronan, G.; Wheeler, D. Lecture presented at the 2nd International Conference on Plasma Source Mass Spectrometry, Durham, UK, 1990.
(37) Bogaerts, A.; Gijbels, R. *J. Appl. Phys.* **1996**, *79*, 1279–1286.
(38) Chapman, B. *Glow Discharge Processes*; Wiley: New York, 1980.

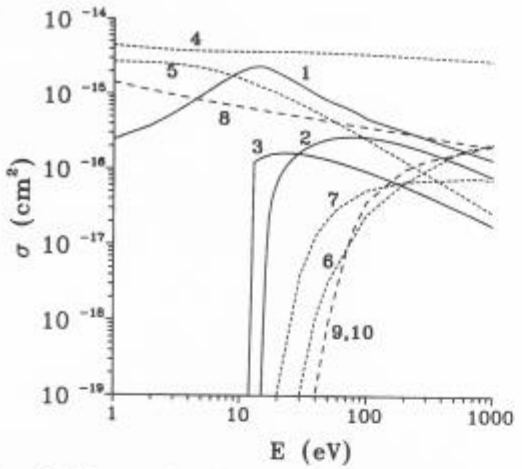

Figure 2. Cross sections of the different collision processes with argon atoms, incorporated in the model, as a function of the particle energies. The solid lines (—) represent electron collisions (1, elastic;[40,41] 2, electron impact ionization;[15] 3, electron impact excitation[39]). The small dashed lines (- - -) represent argon ion collisions (4, charge transfer;[42] 5, elastic;[42] 6, ionization;[43] 7, excitation[43]). The wider dashed lines (– – –) represent the argon atom collisions (8, elastic;[42] 9, ionization;[43] 10, excitation[43]).

processes incorporated in the model are electron impact ionization, excitation, and elastic collisions. The cross sections of these processes as a function of the electron energy are obtained from refs 15, 39–41, and are represented in Figure 2 (solid lines). To determine which kind of collision takes place, the partial collision probabilities are calculated, and the total collision probability is subdivided in intervals with lengths corresponding to these partial probabilities. A second random number is generated, and the interval in which this random number falls determines the kind of collision that takes place. The new energy and three-dimensional direction (azimuthal and axial angles) after collision are also determined by random numbers. After the collision, the electron is followed during the next time step, and the procedure is repeated. In the electron impact ionization collisions, new electrons are created, which are also followed, one after the other. Moreover, by the ion and atom impact ionization processes in the CDS (see below), new electrons are formed as well, which are also introduced into the electron Monte Carlo model. When the electrons in the negative glow (NG) have energies lower than the excitation threshold of argon (~12 eV), they cannot produce inelastic collisions anymore and are hence no longer important as fast electrons. Therefore, they are transferred to the slow electron group at a rate corresponding to a cross section of 10^{-15} cm^2.[26] A more detailed description of the physics and mathematics of this model can be found in refs 25 and 34.

C. Argon Ion and Fast Argon Atom Monte Carlo Model. The argon ions and fast argon atoms are treated with a Monte Carlo model in the CDS. The flux of argon ions starting at the interface between CDS and NG is obtained from the fluid model (see below). The argon ions can also start within the CDS, when they are created by electron impact ionization. Their flux is determined from the fast electron Monte Carlo model (i.e., by the electron impact ionization rates). The ions are followed, one after the other, throughout the entire CDS. Their trajectory is also calculated by Newton's laws (see eqs 1), and the probability of collision is calculated by eq 2. Collision processes taken into consideration are symmetric charge transfer, elastic collisions, and ion impact ionization and excitation. The cross sections of these processes as a function of the ion energy are adapted from refs 42 and 43 and are given in Figure 2 (small dashed lines). In the charge transfer and elastic collisions, fast argon atoms are created. These are also followed throughout the CDS. Their collision processes comprise elastic collisions and atom impact ionization and excitation. The cross sections as a function of the atom energy are also taken from refs 42 and 43 and are presented in Figure 2 (wide dashed lines). In the ion and atom impact ionization processes, new ions are created, which are in turn followed throughout the CDS. For a complete description of this model, see refs 34 and 35.

D. Slow Electron and Argon Ion Fluid Model. The motion of ions and slow electrons is assumed to be collision dominated and described by diffusion and migration in the electric field. The relevant equations are the continuity equations of ions and electrons (eqs 3 and 4, respectively), the flux equations based on diffusion and migration of ions and electrons (eqs 5 and 6, respectively), and the Poisson equation (eq 7):

$$\frac{\delta n_i}{\delta t} + \nabla \cdot j_i = r_i \tag{3}$$

$$\frac{\delta n_e}{\delta t} + \nabla \cdot j_e = r_e \tag{4}$$

$$j_i = -\mu_i n_i \nabla V - D_i \nabla n_i \tag{5}$$

$$j_e = \mu_e n_e \nabla V - D_e \nabla n_e \tag{6}$$

$$\nabla^2 V + \frac{e}{\epsilon_0}(n_i - n_e - n_{e,fast}) = 0 \tag{7}$$

where n_i and n_e are the ion and slow electron densities, j_i and j_e are their fluxes, V is the electrical potential, $n_{e,fast}$ is the fast electron density, which is taken from the electron Monte Carlo model, and r_i and r_e are the creation rates of ions and slow electrons, which also result from the Monte Carlo model. Finally, D_i, D_e, μ_i, and μ_e are the ion and electron diffusion coefficients and mobilities. Their numerical values are assumed to be[26] D_i = 100 cm^2 s^{-1}, $D_e = 2 \times 10^5$ cm^2 s^{-1}, and $\mu_e = 2 \times 10^5$ cm^2 s^{-1} V^{-1} at 1 Torr and 298 K. μ_i is given by the Frost formula:[44]

$$\mu_i = \frac{\mu_{i0}}{\sqrt{1 + a\,|\mathcal{E}/n|}} \tag{8}$$

where $a = 7.36 \times 10^{14}$ cm^{-2} V^{-1}, $\mu_{i0} = 1420$ cm^2 s^{-1} V^{-1} at 1 Torr and 298 K, $\mathcal{E}$ is the electric field, and n is the argon gas atom density.

The five equations can be reduced to three equations by inserting eqs 5 and 6 into eqs 3 and 4, respectively. Boundary

(39) Eggarter, E. *J. Chem. Phys.* **1975**, *62*, 833–847.
(40) Fon, W. C.; Berrington, K. A.; Burke, P. G.; Hibbert, A. *J. Phys. B* **1983**, *16*, 307–321.
(41) de Heer, F. J.; Jansen, R. H. J.; van der Kaay, W. *J. Phys. B* **1979**, *12*, 979–1002.
(42) Phelps, A. V. *J. Appl. Phys.* **1994**, *76*, 747–753.
(43) Phelps, A. V. *J. Phys. Chem. Ref. Data* **1991**, *20*, 557–573.
(44) Frost, L. S. *Phys. Rev.* **1957**, *105*, 354–356.

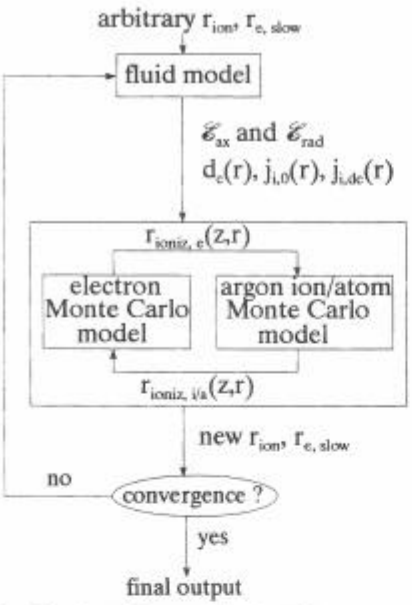

Figure 3. Flow chart of the combined models.

conditions of these equations are $V = -V_c$ at the cathode wall and $V = 0$ at the anode walls, $n_e = 0$ at all walls, and $\nabla n_i = 0$ at all walls.[4] Due to the strong coupling and nonlinearity of these equations, solving the fluid model is a difficult numerical problem. The method we used was developed by Passchier and Goedheer.[3,4] It is a fully implicit method based on the Scharfetter–Gummel exponential scheme for the transport equations.[3–6,45,46] The basic idea is that the particle flux is assumed constant between mesh points, instead of the densities. The advantage of this scheme is its ability to switch between situations where either the drift component or the diffusion component of the particle flux is dominant (i.e., high and low electric field, CDS and NG). More details about the solution method can be found in refs 3, 4, and 34.

E. Combination of the Models. The different models are coupled to each other and solved by an iterative procedure (see Figure 3). The procedure starts with the fluid model, assuming arbitrary ion and slow electron creation rates (r_{ion}, $r_{e,slow}$). Results of the fluid model are, among others, (i) the axial and radial electric field distributions throughout the discharge ($\mathscr{E}_{ax}$ and $\mathscr{E}_{rad}$), (ii) the interface between CDS and NG for all radial positions ($d_c(r)$, defined as the position where the potential goes through zero), (iii) the ion flux entering the CDS ($j_{i,dc}(r)$), and (iv) the ion flux bombarding the cathode ($j_{i,0}(r)$), both as functions of radial position. This information is used in the Monte Carlo models. From the ion flux bombarding the cathode, the electron flux starting at the cathode as a function of the radial position is obtained: $j_{e,0}(r) = -j_{i,0}(r)\gamma$, where γ is the ion-induced secondary electron emission coefficient (see below). The fast electron Monte Carlo model is calculated, as described in section B. This model yields, among others, the ionization rate (i.e., the creation rate of ions) by electron impact as a function of axial and radial positions ($r_{ioniz,e}(z,r)$). This is used in the argon ion and fast atom Monte Carlo model as the number of ions created in the CDS. The ion flux starting at the interface between CDS and NG as a function of radial position is obtained from the fluid model. Outputs of the ion/atom Monte Carlo model are, among others, the ion and atom impact ionization rates (i.e., the creation rate of electrons, $r_{ioniz,i/a}(z,r)$). Next, the fast electron Monte Carlo model is calculated again, incorporating these electrons formed by ion and atom impact ionization. With the new creation rate of ions (i.e., by electron impact ionization), the ion/atom Monte Carlo model is again calculated. This is repeated until convergence is reached (i.e., when the ion flux bombarding the cathode, calculated in the ion/atom Monte Carlo model, does not change anymore). This is generally achieved after two or three iterations.

The creation rate of the slow electrons ($r_{e,slow}$), resulting from the electron Monte Carlo model, and the ion creation rates (r_{ion}), calculated in the fast electron and ion/atom Monte Carlo models, are used as inputs in the fluid model. This yields new axial and radial electric field distributions, a new interface between CDS and NG, and new ion fluxes entering the CDS and bombarding the cathode. This information is again put into the Monte Carlo models. The whole procedure is repeated until final convergence is reached (i.e., generally after 5–10 iterations). The calculations were performed on a Sun Sparcserver 20 workstation. The solution of the coupled equations in the two-dimensional fluid model requires about 3 h, whereas the Monte Carlo models typically take each about 10 min in simulating about 10 000 particles.

RESULTS AND DISCUSSION

Results will be presented for an argon discharge with a copper cathode ($\gamma = 0.083$, from ref 47) at typical discharge conditions of 75 Pa and 1000 V. The gas temperature is assumed to be 360 K.

Figure 4 shows the density profiles of the plasma species. The argon ion density (Figure 4a) is nearly constant (i.e., slightly lower than 10^{10} cm^{-3}) in the CDS but increases rapidly in the NG. Its maximum lies half-way through the discharge (in the axial as well as in the radial directions) and takes a value of about 5.5×10^{11} cm^{-3}. It decreases gradually toward the walls. The slow electron density (Figure 4b) is zero in the CDS and nearly equal to the argon ion density in the NG. This results in a net positive space charge in the CDS and nearly charge neutrality in the NG. Moreover, close to the anode side walls and back plate, the argon ion density is also slightly higher than the slow electron density, resulting in a slight positive space charge there as well. Electron densities have been measured in the literature, and values have been reported of the order of 10^{11} cm^{-3} for a six-way cross glow discharge[48,49] and about 10^{13}–10^{14} cm^{-3} for a Grimm-type glow discharge.[50–53] The Grimm-type discharge operates at much higher pressures and currents, and a higher electron density is therefore expected. Our obtained results are, however, in reasonably good agreement with the values reported for the six-way cross

(45) Gummel, H. K. *IEEE Trans. Electron. Devices* **1964**, *11*, 455–465.
(46) Scharfetter, D. L.; Gummel, H. K. *IEEE Trans. Electron. Devices* **1969**, *16*, 64–77.
(47) Oechsner, H. *Phys. Rev. B* **1978**, *17*, 1052–1056.
(48) Fang, D.; Marcus, R. K. *Spectrochim. Acta* **1990**, *45B*, 1053–1074.
(49) Fang, D.; Marcus, R. K. *Spectrochim. Acta* **1991**, *46B*, 983–1000.
(50) Büger, P. A. Z. *Naturforsch. A* **1975**, *30*, 216–222.
(51) Ferreira, N. P.; Human, H. G.; Butler, L. R. P. *Spectrochim. Acta* **1980**, *35B*, 287–295.
(52) Kuraica, M.; Konjevic, N.; Platisa, M.; Pantelic, D. *Spectrochim. Acta* **1992**, *47B*, 1173–1186.
(53) Bogaerts, A.; Quentmeier, A.; Jakubowski, N.; Gijbels, R. *Spectrochim. Acta* **1995**, *50B*, 1337–1349.

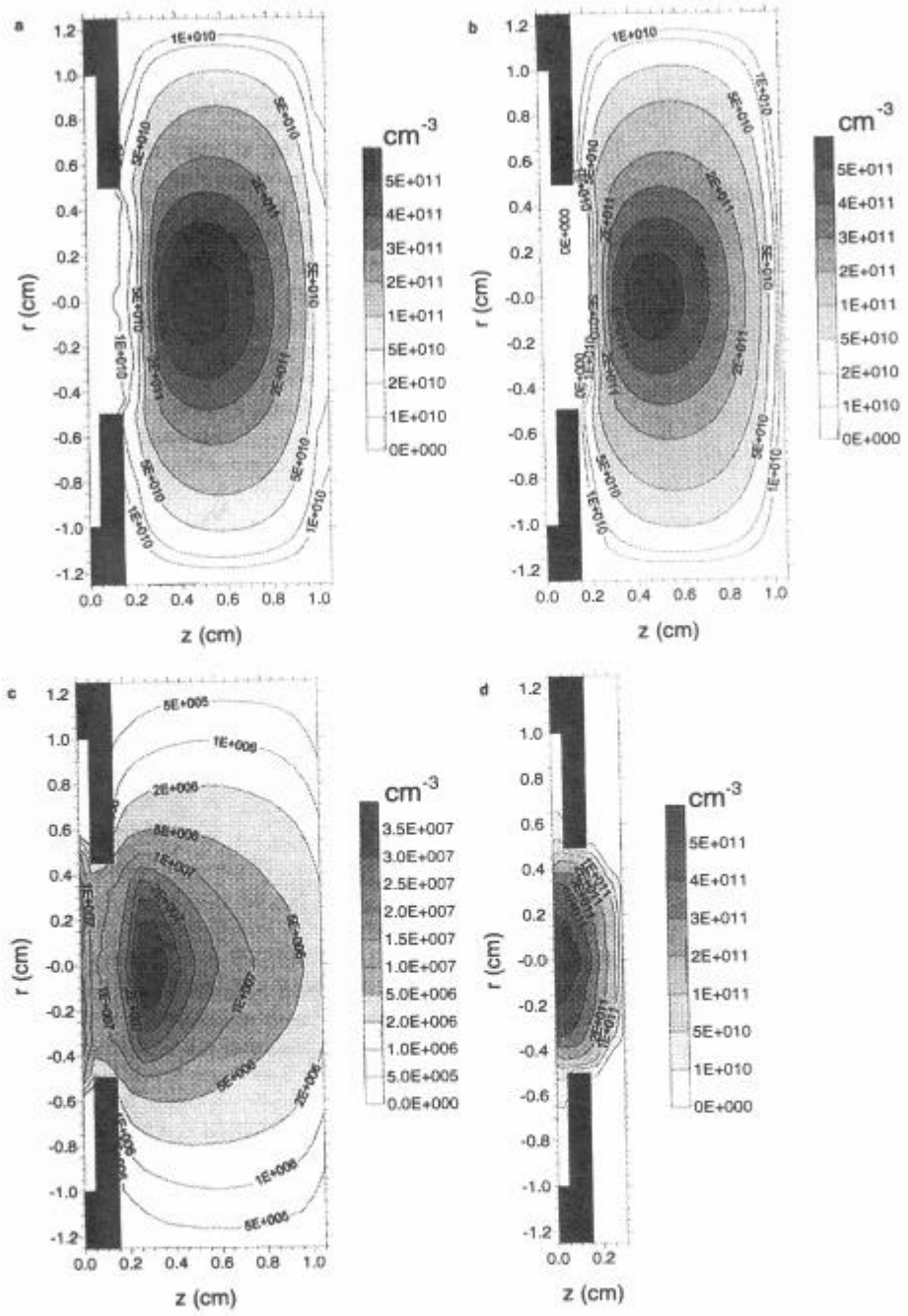

Figure 4. Density profiles of the argon ions (a), slow electrons (b), and fast electrons (c) throughout the discharge and of the fast argon atoms (d) in the CDS at 75 Pa, 1000 V, 3.4 mA.

glow discharge, which operates at more or less similar discharge conditions. The fast electron density (Figure 4c) reaches a maximum slightly closer to the cathode and is about 4 orders of magnitude lower than the argon ion and slow electron densities. Hence, it does not contribute to the space charge. The fast argon atom density (Figure 4d, only presented in the CDS since its density is zero in the NG) reaches a maximum of about 6×10^{11} cm^{-3} close to the cathode. The density of the fast argon atoms is negligible compared to the overall argon atom density (i.e., $\sim 1.5 \times 10^{16}$ cm^{-3}), so it can be said that the argon gas is more or less at rest. It can be seen in Figure 4 that the calculated species densities are almost zero behind the front plate (see Figure 1 for the position of the front plate). Indeed, this region does not really take part in the glow discharge plasma, since the distance between cathode and front plate is smaller than one CDS length (which is the necessary condition for a glow discharge to be created).

Figure 5 shows the potential distribution throughout the discharge. The potential is −1000 V at the cathode. It increases rapidly in the CDS and reaches zero about 0.24 cm from the cathode. This is defined as the interface between CDS and NG.

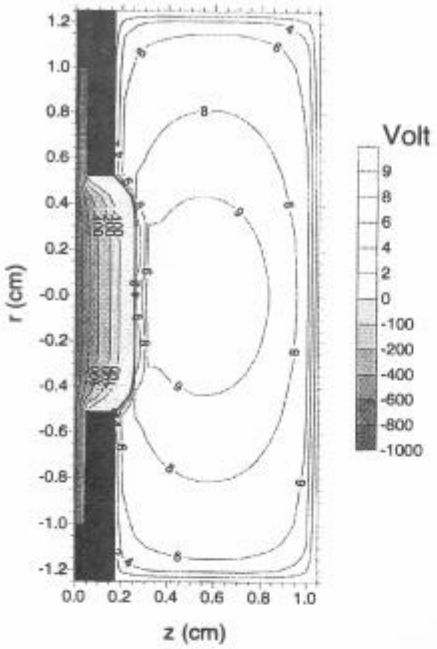

Figure 5. Potential distribution throughout the discharge at 75 Pa, 1000 V, 3.4 mA.

Hence, the total voltage applied to the glow discharge cell falls off in the CDS. Since the front plate of the cell is also at anode potential, and since the charged particle densities are almost zero behind the front plate (see Figure 4), the potential drops nearly linearly in this region. The potential reaches a small positive value in the NG (of the order of 9.5 V at maximum), which is called the plasma potential, and returns to zero at the anode side walls and back plate. Hence, the plasma does not take a potential intermediate between cathode and anode but is the most positive region of the discharge.

Figure 6, parts a and b, represents the axial and radial electric fields, respectively. Due to the large potential drop in the CDS, the axial field (Figure 6a) in this region is rather high. It reaches values of about −7.5 kV/cm at the cathode and decreases almost linearly toward the NG. It goes through zero half-way through the discharge and increases again to slightly higher than 200 V/cm at the anode back plate. There is almost no radial gradient in the axial electric field in the NG, i.e., the axial electric field is only a function of the axial position. Behind the front plate, a very high axial electric field is observed, due to the large potential drop over a very short distance. The radial electric field (Figure 6b) is rather high close to the front plate due to the large potential drop between cathode and front plate. It reaches values of about −10 kV/cm very close to the front plate and decreases rapidly toward the cell axis. At about 0.1 cm from the cell axis, the radial electric field takes slightly positive values in the CDS (20 V/cm at maximum). It decreases again to zero at the cell axis. In the NG, the radial electric field is only small, but it increases toward the side walls, reaching values of about 100 V/cm at the walls. Similarly, there is almost no axial gradient in the radial electric field in the NG, except close to the anode back plate. Generally, the electric fields at the cell walls (i.e., about −7.5 kV/cm at the cathode, and about 100 V/cm at the anode walls) are such as to repel electrons trying to reach the walls.

Figure 7 shows the mean energies of the plasma species. The electrons (Figure 7a) start at the cathode with energies of about 4 eV. They move away from the cathode, thereby gaining energy from the electric field. At the same time, they will lose energy by inelastic collisions, so that their energy will not be equal to the total potential drop (i.e., 1000 V) at the CDS−NG interface but reaches a maximum value of about 500 eV at the end of the CDS. In the NG, the electrons do not gain much energy from the weak electric field anymore; on the contrary, they lose their energy more efficiently by collisions, so that their mean energy decreases again to about 300−400 eV. It is more or less the same

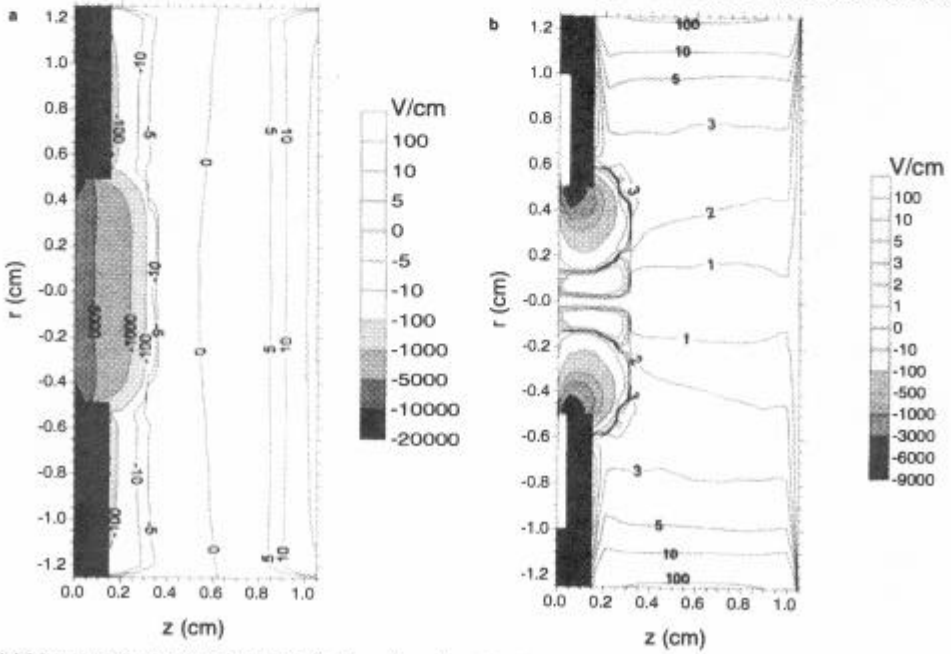

Figure 6. Axial (a) and radial (b) electric field distributions throughout the discharge at 75 Pa, 1000 V, 3.4 mA.

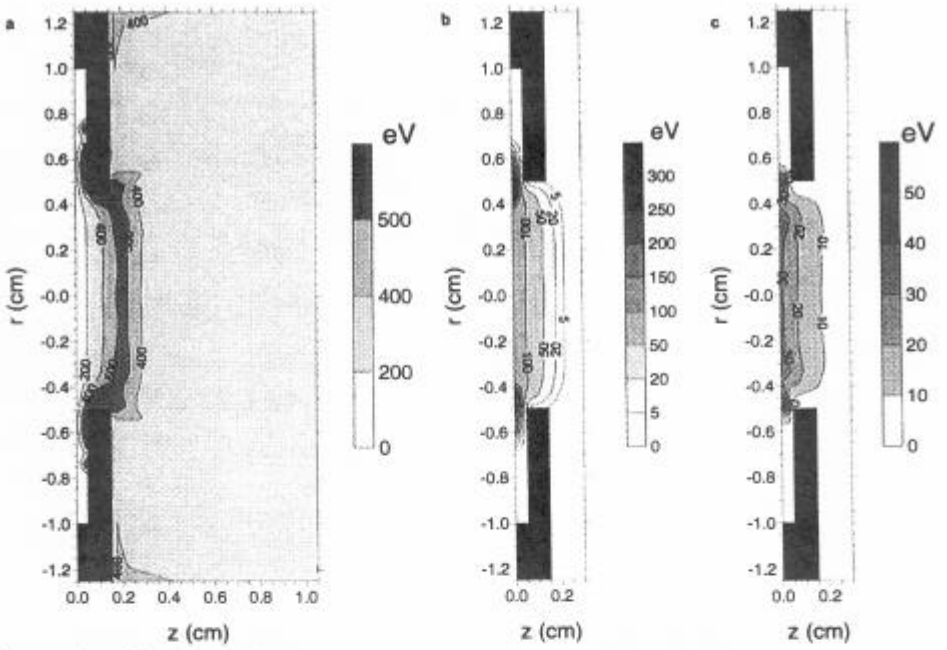

Figure 7. Mean energies of the electrons throughout the discharge (a) and of the argon ions (b) and fast argon atoms (c) in the CDS at 75 Pa, 1000 V, 3.4 mA.

in the entire NG, due to the back-and-forth scattering of the electrons in this region. Figure 7, parts b and c, presents the mean energies of the argon ions and fast argon atoms, respectively. Only the CDS is shown, since these species are more or less thermalized in the NG. The mean energies are almost zero at the CDS–NG interface and increase gradually toward the cathode. The mean energy of the ions reaches values of about 150 eV at the cathode. This is clearly lower than the mean energy of the electrons at the CDS–NG interface, in spite of the fact that both species gain the same amount of energy from the electric field. This indicates that the argon ions lose their energy much more efficiently by collisions than the electrons. Indeed, the symmetric charge transfer collisions are more frequent than the electron impact ionization and excitation collisions (i.e., larger cross section, see Figure 2) and lead to a stronger energy loss (i.e., the argon ions that have undergone a charge transfer collision start again with zero energy[25]). Near the front plate, the ions can reach higher energies (300 eV at maximum), since they take up more energy from the strong electric field without losing much energy over such short distances. The fast argon atoms (Figure 7c) still have lower mean energies than the argon ions, since they are formed out of the ions (they take over their energy in charge transfer collisions), but they are not able to gain more energy from the electric field. It is seen on the figure that these fast atoms can reach maximum energies at the cathode of about 35 eV at the cell axis to about 50 eV near the front plate. It should be borne in mind that the term "fast atoms" is used for those atoms with energies beyond 1 eV. Atoms with energies below 1 eV are assumed to belong to the thermalized group.

The Monte Carlo models also give information about the relative importance of the different collision processes. The electron impact ionization rate (Figure 8a) reaches a maximum of about 7×10^{16} cm^{-3} s^{-1} in the beginning of the NG on the cell axis. Most of the argon ions are hence created by electron impact at the center of the plasma. The rates of electron impact excitation and elastic collisions (both not presented here) are characterized by the same profile, but the excitation rate is only half as high, whereas the elastic collision rate is about 6 times higher, as expected from the cross sections (Figure 2). The most important collision processes of the argon ions are symmetric charge transfer collisions. The charge transfer collision rate is about 3×10^{17} cm^{-3} s^{-1} at the CDS–NG interface and increases gradually toward the cathode, taking values of about 1.5×10^{18} cm^{-3} s^{-1} close to the cathode. The rate of elastic collisions is at maximum ($\sim 4 \times 10^{17}$ cm^{-3} s^{-1}) at the CDS–NG interface, where the ion energies are low, and it decreases to about 5×10^{16} cm^{-3} s^{-1} close to the cathode. The elastic collision rate of the fast argon atoms is about 10^{18}–10^{19} cm^{-3} s^{-1} in the CDS, reaching a maximum close to the cathode, where the fast argon atom density is at its maximum (see Figure 4d). The ionization rates by argon ions and fast argon atoms are presented in Figure 8, parts b and c, respectively. The excitation rate by these species is comparable to the ionization rate and is not shown. As is illustrated in Figure 2, the ion/atom impact ionization cross section increases with energy. Therefore, the ionization rate is low at the CDS–NG interface and increases toward the cathode. Close to the cathode, it is of the order of $(1–1.5) \times 10^{16}$ cm^{-3} s^{-1} for the argon ions and of the order of $(7–9) \times 10^{16}$ cm^{-3} s^{-1} for the fast argon atoms. Hence, these processes are only of minor importance for the ions and atoms compared to the charge transfer and elastic collisions. However, compared to the electron impact ionization rate, these processes are not negligible, especially close to the cathode. When we integrate the ionization rates by electrons, argon ions, and argon atoms over the total discharge region, the relative importance of these processes to the total ionization of argon can be obtained. This was calculated to be about 89% for the electrons (about 15% in the CDS and about 74% in the NG), about 2.5% for the argon ions, and about 8.5% for the fast argon atoms. Although electron

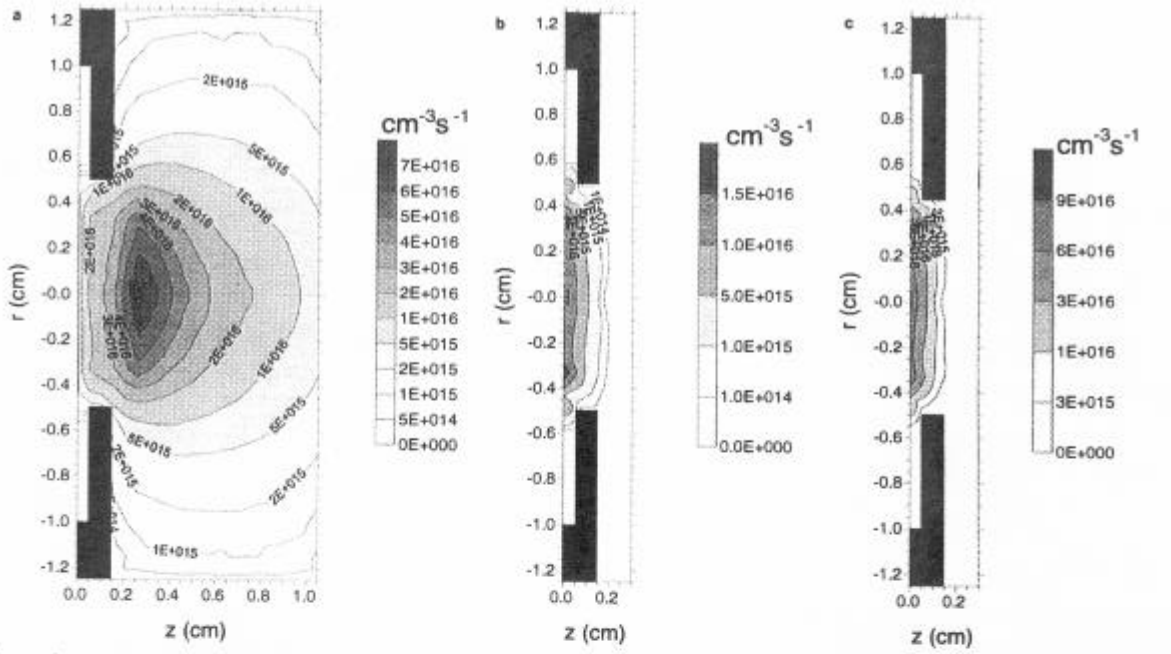

Figure 8. Argon ionization rates by the electrons throughout the discharge (a) and by the argon ions (b) and fast argon atoms (c) in the CDS at 75 Pa, 1000 V, 3.4 mA.

impact ionization is clearly dominant, argon ion and atom impact ionizations are not negligible at these discharge conditions. It was demonstrated before[35] that, at discharge voltages above 600 V, the correct voltage–current characteristics of the glow discharge can be obtained only by the incorporation of these processes.

The models described in this work were developed earlier in one dimension,[25,35,36] i.e., the fluid model was one-dimensional, but the Monte Carlo models were already in three dimensions (but without radial electric field yet). We compared the results of the two-dimensional model (values taken at the cell axis) with the one-dimensional results at the same pressure, voltage, and gas temperature and found that the results were rather similar, except that the argon ion and slow electron densities are slightly lower in the two-dimensional case.

Finally, for the given voltage and pressure of 1000 V and 75 Pa, the total electrical current was calculated to be 3.4 mA at a gas temperature of 360 K. These voltage–pressure–current values are in good agreement with experiment, which indicates that the present models give more or less realistic results.

CONCLUSION

A two-dimensional model is developed to describe a direct current glow discharge in argon. It is a hybrid model, consisting of (i) a Monte Carlo model for the fast electrons in the entire discharge, (ii) a Monte Carlo model for the argon ions and fast argon atoms in the CDS, and (iii) a fluid model for the argon ions and slow electrons in the entire discharge. Typical results of these models include the particles densities and mean energies, the potential distribution, the axial and radial electric field, and the rates of the different collision processes, all as a function of axial and radial position. Moreover, from the given pressure, voltage, and gas temperature, the total electrical current was calculated and showed good agreement with experiment.

The present model describes only the electrons, argon ions, and fast argon atoms (so-called plasma model) and not yet the sputtered (analytically important) species. However, as is shown in ref 37 for one dimension, the results of the plasma model are important for describing the sputtered species and must, therefore, be calculated first. Indeed, the electric field distribution is used for calculating the behavior of the ions of the sputtered species (migration in the electric field), the argon ion and fast atom flux and energy at the cathode determine the amount of sputtering, the electron flux and energy are used to compute the amount of electron impact ionization of the sputtered atoms, and the argon ion density distribution is required to calculate the amount of charge transfer ionization of the sputtered atoms. In a later work, the results obtained in the present paper will be used for describing the sputtered species in two dimensions.[54]

ACKNOWLEDGMENT

A.B. is supported by the Belgian National Fund for Scientific Research (NFWO). The authors also acknowledge financial support from the Federal Services for Scientific, Technical and Cultural Affairs (DWTC/SSTC) of the Prime Minister's Office through IUAP-III (Conv. 49). Finally, they thank A. V. Phelps for the interesting discussions about the collision cross sections.

Received for review October 24, 1995. Accepted April 8, 1996.*

AC9510651

(54) Bogaerts, A.; Gijbels, R. *Anal. Chem.* (submitted).

* Abstract published in *Advance ACS Abstracts*, May 15, 1996.